Dehydration, Hydration Behavior, and Structural Analysis of Fenoprofen Calcium

HAIJIAN ZHU, JIA XU, PETER VARLASHKIN, STACEY LONG, CHRIS KIDD

Pharmaceutical Development Discovery and Analytical Sciences Departments, Glaxo Wellcome Inc., Five Moore Drive, Research Triangle Park, North Carolina 27709

Received 16 May 2000; revised 4 December 2000; accepted 8 December 2000

ABSTRACT: Fenoprofen calcium (FC) is a nonsteroidal, anti-inammatory, analgesic, and antipyretic agent. The dehydration behavior of FC dihydrate and the rehydration of the dried FC were investigated using differential scanning calorimetry (DSC), thermogravimetric analysis (TGA), and powder X-ray diffractometry (PXRD). The stoichiometry, the crystal packing arrangement, and water environments in FC dihydrate were determined using single-crystal X-ray diffraction (XRD) analysis. The Arrhenius plot (natural logarithm of the dehydration rate constant versus the reciprocal of absolute temperature) for FC dihydrate from isothermal TGA is not linear. The activation energy of dehydration was 309 kJ/mol in the 50 60 °C range and 123 kJ/mol in the 60 80 °C range. The difference in activation energy can be explained from the crystal structure data where one water molecule is sandwiched between repeating polar carboxylate groups and the other water is in a slightly less polar region of the crystal. Single-crystal XRD analysis also indicated each calcium ion is coordinated to six oxygens. Two coordinating oxygens are provided by two water molecules and the other four oxygens are provided by the carboxylate group of four separate fenoprofen anions. Each fenoprofen anion, which can provide two oxygens for coordination, is associated with two different calcium ions. Hot-stage PXRD suggested that only a loss of 1 mole of water per mole of FC dihydrate (forming a monohydrate) was required to convert the material to a partially crystalline state. The monohydrate is not completely disordered as evidenced by a strong diffraction peak as well as some weaker peaks in the PXRD pattern. The rehydration of the anhydrous form of FC follows a solution-mediated transformation, prior to crystallizing as the dihydrate. J Pharm Sci 90:845 859, 2001
Keywords: fenoprofen calcium XRD; PXRD; TGA; DSC

INTRODUCTION

Salts are usually considered alternatives when the physicochemical characteristics of the parent drug molecules are unsuitable or inadequate for satisfactory formulations. Considerable variation in solubility, dissolution rate, bioavailability, and other pharmaceutically important properties can result from the association of the drug with different salt forming counterions.[1] Furthermore, because of lack of predictive relationships between the physicochemical properties of the resultant salts, the selection of an appropriate salt form with desired combination of properties can be a difcult, semi-empirical choice.

Pharmaceutical salts frequently exist as hydrates. Because the nature and stability of a salt hydrate are known to vary with a change of the counterion,[2] knowledge of the stoichiometry and nature of the binding environment of water in the salt hydrate is essential for optimum salt selection.

This work is presented in memory of one of the authors, Jia Xu.

Correspondence to: P. Varlashkin (Telephone: 919-483-8464; Fax: 919-315-1091; E-mail: PGV48846@glaxowellcome.com)

Journal of Pharmaceutical Sciences, Vol. 90, 845 859 (2001)

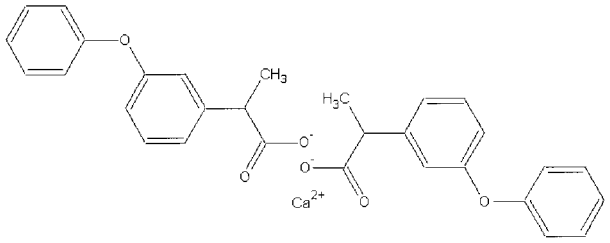

Figure 1. Molecular structure of fenoprofen calcium.

Fenoprofen calcium (calcium methyl-3-phenoxybenzeneacetate, Figure 1) is a nonsteroidal, antiinflammatory, analgesic, and antipyretic agent.[3] Fenoprofen calcium (FC) was reported to exist as a monohydrate and a dihydrate.[4,5] Some physicochemical data of those hydrates are available.[4,5] In this study, we describe the use of thermal analysis and hot stage/environmentally controlled X-ray diffraction analysis (XRD) to study the dehydration and rehydration behavior of FC. The crystal structure of FC dihydrate is reported here for the first time and is used to confirm the stoichiometry of water to FC and to provide insight into the dehydration behavior of FC dihydrate.

EXPERIMENTAL SECTION

Materials

FC dihydrate (MW = 558.64 g/mol) was purchased from the Sigma Chemical Company. The material was confirmed as the dihydrate reported previously[4,5] through physical characterization using powder X-ray diffraction (PXRD), Karl-Fischer titrimetry, differential scanning calorimetry (DSC), and thermogravimetric analysis (TGA).

Preparation of Single Crystals and Structure Determination of FC Dihydrate

The single crystal of FC dihydrate was prepared by gradually cooling a saturated FC aqueous solution from 60°C to room temperature. Wet crystals were submitted to the X-ray Crystallographic Facility at the Chemistry Department, University of North Carolina (UNC), Chapel Hill, NC. The 2θ and intensity data were collected at − 100 °C using a Bruker SMART diffractometer. Unit cell dimensions were obtained from 6683 reflections. Structure solution and refinement was based on 2466 unique and significant reflections ($R_f = 0.062$ and $R_w = 0.064$). The program used for data reduction and analysis has been described.[6] UNC single-crystal structure results were reported to the authors in UNC Single Crystal X-ray Facility report number c99083. The unit cell and atomic coordinate information is provided in Table 1.

Differential Scanning Calorimetry (DSC)

A TA 2910S differential scanning calorimeter equipped with a data station (TA Instruments, New Castle, DE) was used to determine the thermal behavior of the FC dihydrate. The temperature axis and the cell constant of the DSC cell were calibrated with indium. Sample (~5 mg) in a crimped aluminum pan was heated at 10 °C/min under a nitrogen purge at 40 mL/min.

Thermogravimetric Analysis (TGA)

The TGA curves were obtained using a TA Hi-Res 2950 thermogravimetric analyzer linked to a data station (TA Instruments, New Castle, DE). Isothermal TGA was performed on samples (10 mg) in open aluminum pans at 50, 55, 60, 70, and 80 °C with a nitrogen purge at 60 mL/min.

Karl Fischer Titrimetry (KFT)

The amounts of water in the FC dihydrate were determined using a Moisture Meter (Mitsubishi CA-05, Mitsubishi Chemical Industries Ltd., Tokyo, Japan). Sample was weighed and quickly transferred to the titration vessel containing anhydrous methanol prior to titration.

Powder X-ray Diffraction (PXRD)

The powder X-ray diffractometer and an "in-house" built environmental sample chamber have been described.[7] For the dehydration study, scans were collected at 4 degrees 2θ/min at a digital resolution of 0.03 degrees 2θ using copper Kα radiation while drying the covered sample at 50°C under a stream of dry nitrogen. The sample cover uses a X-ray transparent window. XRD peak integration was performed by removing background and then integrating using the BACKGROUND and AREA programs, respectively, of Scintag's DMS software, v. 3.35.

Two series of experiments were conducted to qualitatively examine the dehydration/rehydration of FC dihydrate. One series of experiments utilized a Baxter DP-32 vacuum drying oven to

Table 1. Single-Crystal X-ray Diffraction Unit Cell and Atomic Coordinates[a]

	Fraction Atomic Coordinate			
Atom	x	y	z	Biso[b]
Cal	0.98906 (6)	0.74938 (15)	0.02478 (6)	2.71 (4)
O1	0.96583 (20)	0.5070 (5)	− 0.07293 (20)	3.89 (19)
O2	0.94168 (22)	0.7794 (4)	− 0.090053 (21)	4.45 (22)
C3	0.9440 (3)	0.6259 (9)	− 0.1127 (3)	3.5 (3)
C4	0.9244 (4)	0.5832 (8)	− 0.1857 (4)	5.3 (4)
C5	0.9030 (5)	0.7314 (10)	− 0.2280 (4)	7.4 (4)
C6	0.8723 (4)	0.4315 (8)	− 0.1924 (4)	4.2 (3)
C7	0.8739 (4)	0.3289 (9)	− 0.2490 (4)	4.6 (3)
C8	0.8272 (4)	0.1897 (8)	− 0.2574 (4)	5.2 (4)
C9	0.7793 (4)	0.1528 (9)	− 0.2081 (5)	5.5 (4)
C10	0.7776 (3)	0.2564 (11)	− 0.1522 (4)	5.4 (4)
C11	0.8242 (4)	0.3965 (8)	− 0.1436 (4)	5.1 (4)
O12	0.7283 (3)	0.2352 (8)	− 0.1025 (3)	9.2 (4)
C13	0.7059 (5)	0.0722 (14)	− 0.0863 (4)	6.7 (5)
C14	0.6371 (6)	0.0457	− 0.0801 (5)	9.0 (7)
C15	0.6124 (10)	− 0.116 (3)	− 0.0596 (10)	13.5 (14)
C16	0.6566 (14)	− 0.239 (3)	− 0.0454 (11)	16.6 (18)
C17	0.7281 (11)	− 0.2197 (19)	− 0.0499 (6)	13.3 (11)
C18	0.7531 (6)	− 0.0584 (18)	− 0.0727 (5)	9.1 (6)
O21	1.10105 (21)	0.7213 (5)	− 0.02755 (24)	4.90 (23)
O22	1.07599 (19)	0.9950 (5)	− 0.03653 (21)	4.03 (20)
C23	1.1105 (3)	0.8677 (8)	− 0.0536 (3)	3.9 (3)
C26	1.1789 (6)	0.7275 (10)	− 0.1468 (6)	8.1 (6)
C27	1.2352 (5)	0.6200 (11)	− 0.1353 (4)	7.4 (5)
C28	1.2431 (4)	0.4748 (9)	− 0.1772 (5)	6.0 (4)
C29	1.1977 (5)	0.4376 (9)	− 0.2284 (4)	5.9 (4)
C30	1.1421 (5)	0.5490 (11)	− 0.2391 (5)	7.2 (5)
C31	1.1329 (6)	0.6917 (11)	− 0.1983 (6)	7.9 (6)
O32	1.0943 (5)	0.5298 (10)	− 0.2918 (5)	11.8 (6)
C33	1.0826 (5)	0.3692 (16)	− 0.3228 (6)	7.4 (6)
C34	1.0604 (6)	0.2359 (22)	− 0.2846 (6)	9.8 (7)
C35	1.0445 (7)	0.078 (3)	− 0.3161 (11)	12.8 (12)
C36	1.0545 (8)	0.0677 (22)	− 0.3839 (12)	13.1 (12)
C37	1.0770 (7)	0.199 (3)	− 0.4238 (7)	11.3 (10)
C38	1.0907 (4)	0.3511 (17)	− 0.3898 (7)	8.0 (7)
O41	1.03566 (21)	0.8856 (5)	0.12680 (20)	4.48 (20)
O42	0.88541 (22)	0.6075 (5)	0.0586 (3)	6.8 (3)
C241	1.1849	0.8738 (15)	− 0.0856 (6)	2.70 (22)
C251	1.1889 (7)	1.0466 (18)	− 0.1306 (7)	4.2 (3)
C242	1.1511 (7)	0.8968 (17)	− 0.1195 (7)	4.0 (3)
C252	1.2149 (7)	1.0173 (17)	− 0.0988 (7)	3.8 (3)
H4	0.967	0.542	− 0.206	6.0
H5a	0.893	0.694	− 0.274	8.2
H5b	0.861	0.779	− 0.209	8.2
H5c	0.939	0.818	− 0.228	8.2
H7	0.908	0.353	− 0.283	5.3
H8	0.828	0.121	− 0.299	5.9
H9	0.748	0.056	− 0.213	6.3
H11	0.822	0.467	− 0.103	5.9
H14	0.605	0.139	− 0.090	9.8
H15	0.563	− 0.136	− 0.057	14.3
H16	0.637	− 0.348	− 0.032	17.5
H17	0.759	− 0.313	− 0.037	14.1

Table 1. (*Continued*)

	Fraction Atomic Coordinate			
Atom	x	y	z	Biso[b]
H18	0.803	− 0.040	− 0.079	9.9
H27	1.268	0.644	− 0.099	8.3
H28	1.282	0.398	− 0.169	6.8
H29	1.204	0.339	− 0.258	6.8
H31	1.094	0.768	− 0.207	8.8
H34	1.056	0.250	− 0.236	10.7
H35	1.027	− 0.018	− 0.290	13.6
H36	1.045	− 0.043	− 0.405	13.8
H37	1.082	0.188	− 0.472	12.1
H38	1.108	0.450	− 0.414	8.8
H41b	1.079	0.857	0.151	5.2
H41a	1.047	1.006	0.121	5.2
H42a	0.853	0.604	0.096	7.7
H42b	0.836	0.633	0.053	7.7
H241	1.225	0.856	− 0.053	3.7
H251a	1.237	1.054	− 0.149	4.7
H251b	1.156	1.046	− 0.165	4.7
H251c	1.185	1.145	− 0.100	4.7
H242	1.122	0.956	− 0.155	4.8
H252a	1.243	1.045	− 0.138	4.9
H252b	1.199	1.126	− 0.079	4.9
H252c	1.245	0.960	− 0.065	4.9

[a]UNC report code c99083; space group and cell dimensions: monoclinic, $P2_1/n$; $a = 18.9996(8)$, $b = 7.7270(3)$, $c = 19.4811(9)$ Å; beta = 91.530(1)°; unit cell volume = 2859.00 (21) Å cubed; FW = 558.64 g/mol; Z (# molecules in unit cell) = 4; calculated density = 1.298 g/cc. (ESDs refer to the last digit printed)

[b]Biso is the mean of the principal axes of the thermal ellipsoid.

dehydrate the FC dihydrate and an Espec LHU-112 humidity cabinet set at 40 °C/75% relative humidity (RH) to rehydrate the material. FC dihydrate was mounted on a silicon zero background wafer, and the initial PXRD pattern was collected. The sample was then placed in the vacuum drying oven and dried at 70°C under vacuum. A second PXRD pattern was collected of the dehydrated material. The sample was placed in the humidity cabinet and periodically removed and scanned. Visual observations were also recorded.

A second series of dehydration/rehydration experiments were performed *in situ* using a hot stage/environmental chamber[7] designed for the Scintag XDS2000. FC dihydrate was mounted on a silicon wafer and placed in the hot stage/environmental chamber. An initial PXRD pattern was recorded and then the hot stage was set to 70°C and a dry stream of nitrogen (350 mL/min) was blown into the environmental chamber. Scans were collected continuously until the diffraction patterns indicated the dihydrate had fully dehydrated, as confirmed by TGA. The hot stage was lowered to 40°C, and a RH100 humidity generator (VTI Corp., Hialeah, FL) was utilized to produce a 75% RH atmosphere in the chamber. The humidifier on the RH100 was set at 55°C, and the heated transfer line between the generator and environmental chamber was set at 45°C. The flow rate of moist nitrogen from the RH100 was 350 mL/min. A heat lamp equipped with a dimmer helped maintain the temperature inside the chamber at 40°C. PXRD scans were collected periodically.

Cerius2 Modeling

Single-crystal structure data were imported into Cerius2 (Molecular Simulations, Inc.), v. 3.9 to provide visualization of the crystal structure and calculation of the simulated PXRD pattern. For atomic charge assignments and energy minimizations, the Charge Equilibrium method and Dreiding v. 2.21 and Universal v. 1.02 force fields were used, respectively.

RESULTS AND DISCUSSION

Dehydration Kinetics by Isothermal TGA

The weight loss, expressed as fraction dehydrated, x, was obtained at fixed temperatures covering the range 50 to 80°C maximum possible weight loss of water in dehydrating the fenoprofen calcium. Therefore, 100% fraction dehydrated ($x = 1$) corresponds to the loss of two water molecules of hydration. Prior to each isothermal scan, the TGA furnace was rapidly heated to the required study temperature and the samples were maintained at that temperature until dehydration was complete. The fraction dehydrated, x, was plotted as a function of time, t, according to the kinetic models of the reaction mechanisms known to occur in the solid state.[8–10] The correlation coefficient squared, r^2, was determined to test the extent of conformity of the data to the kinetic models. The activation energies of dehydration were determined from Arrhenius plots of the rate constant derived from the statistically best fitting mechanism.

Typical isothermal dehydration plots are shown in Figure 2. In all temperatures, the shape of the curve is sigmoidal and the dehydration rate increases with temperature. The dehydration curves were fitted by various rate equations (see Table 2). The dehydration kinetics was best described by the three-dimensional growth of nuclei equation (eq. A3) or the three-dimensional phase boundary equation (eq. R3). The activation energies evaluated by graphical solutions of Arrhenius equation using the rate constant calculated from either equation was ~309 kJ/mol for the temperature range 50–60°C and 123 kJ/mol for the temperature range 60–80°C (Table 3 and Figure 3). Because the sample presentation, surface area, bulk density, particle size, flow rate, and RH of the drying stream, etc. may affect dehydration rate, it is not surprising that the rate constants obtained in this work do not agree with the results by Sathe and Moore[4] (i.e., 0.02 versus 0.04 h^{-1} at 50°C, respectively). Interestingly, even though the prior work of Sathe and Moore did not mention two possible dehydration modes, their Arrhenius plot (natural logarithm of the dehydration

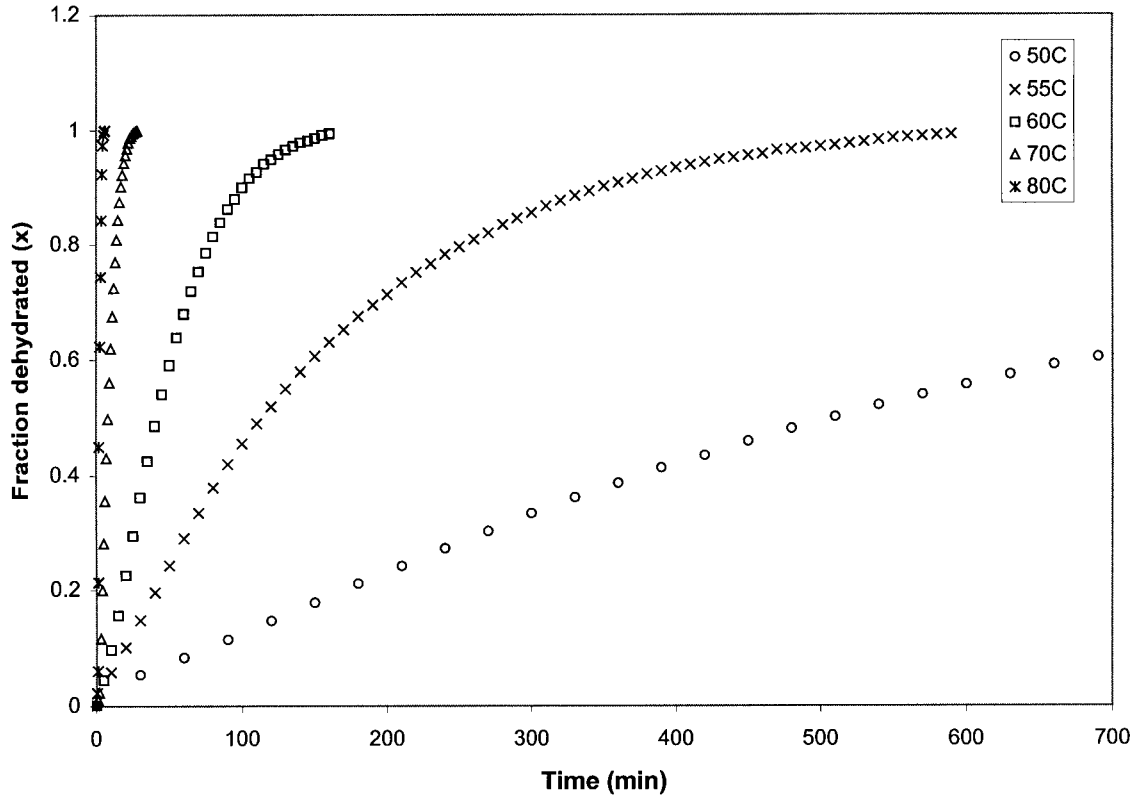

Figure 2. Plot of fraction dehydrated against time for the dehydration of FC dihydrate under isothermal conditions.

Table 2. Kinetic Equations of the Most Common Mechanism of Solid-State Decompositions[8] and Correlation Coefficients Squared (r^2) of Isothermal TGA Data Fitting

Symbol	Equation	Rate-Controlling Process	r^2
P1	$\ln[x/(1-x)] = kt$	Random nucleation (Prout–Tompkins equation)	0.9620
A2	$[-\ln(1-x)]^{1/2} = kt$	Two-dimensional growth of nuclei (Avrami–Erofeev, $n = 1/2$)	0.9764
A3	$[-\ln(1-x)]^{1/3} = kt$	Three-dimensional growth of nuclei (Avrami–Erofeev, $n = 1/3$)	0.9915
F1	$-\ln(1-x) = kt$	Random nucleation (first-order mechanism)	0.9439
R1	$x = kt$	One-dimensional phase boundary reaction (zero-order mechanism)	0.8102
R2	$[1-(1-x)]^{1/2} = kt$	Two-dimensional phase boundary reaction (zero-order mechanism)	0.9788
R3	$[1-(1-x)]^{1/3} = kt$	Three-dimensional phase boundary reaction (spherical symmetry)	0.9919
D1	$x^2 = kt$	One-dimensional diffusion	0.9388
D2	$(1-x)\ln(1-x) + x = kt$	Two-dimensional diffusion	0.9568
D3	$[1-(1-x)^{1/3}]^2 = kt$	Three-dimensional diffusion (Jander equation)	0.9126
D4	$1-(2/3)x-(1-x)^{2/3} = kt$	Three-dimensional diffusion (Ginstling–Brounshtein equation)	0.7992

rate constant versus the inverse of the absolute temperature) suggests a break that may indicate two "modes" of dehydration process as pointed out in this paper. The calculated activation energies from the data by Sathe and Moore[4] at two different temperature ranges 50–60 and 60–80°C are 345 and 135 kJ/mol, respectively, and are comparable with the data in this work. The difference in the activation energies for the two temperature ranges is due to the different water environments in FC dihydrate, as confirmed by the single-crystal XRD analysis.

Dehydration Kinetics by PXRD

Figure 4 shows the PXRD pattern of FC dihydrate over time when exposed to 50°C. Over a period of a few hours, the diffraction peaks for the crystalline dihydrate are reduced in intensity followed by the growth of a low angle diffraction peak (5° 2θ). Qualitatively, the dehydration seems to follow the loss of the crystalline dihydrate phase followed by the formation of a partially crystalline phase. The simply ordered phase is not purely amorphous because of the presence of a strong diffraction peak, as well as some minor peaks (Figure 4). After the diffraction peaks of the crystalline dihydrate were not detectable, the drying experiment was stopped and the residual moisture in the dried sample on the XRD environmental stage was immediately determined by KFT. The sample contained ~3.8 % water, which corresponds to a FC monohydrate.

Table 3. Dehydration Rate Constants by Fitting the Isothermal TGA Data to the Three-Dimensional Phase Boundary Equation

Temperature (°C)	Dehydration Rate Constant (k, min^{-1})
50	0.0003
55	0.0013
60	0.0090
70	0.0422
80	0.1129

The PXRD pattern of a crystalline powder is characteristic of the crystal lattice of that particular compound, including a hydrate. By measuring the rate of disappearance (or appearance) of a peak unique to the hydrate (or dehydrated form), the kinetics of the solid-state dehydration can be determined. Consider a mixture of FC dihydrate (A) and monohydrate (B). The intensity of PXRD peak of the ith diffraction line of the dihydrate (A) component is given in eq. 1:

$$I_{iA} = (k_{iA}X_A)/\mu^*_{mat} \quad (1)$$

where I_{iA} is the intensity of the ith diffraction peak of component A, X_A is the weight fraction of component A, μ^*_{mat} is the mass absorption coefficient for the total matrix (A + B), k_{iA} is a constant containing instrumental factors, atomic factors, and the density of A. The value of k_{iA} is dependent on the chosen diffraction peak.

Similarly, the intensity of the X-ray powder diffraction peak of the jth diffraction line of the

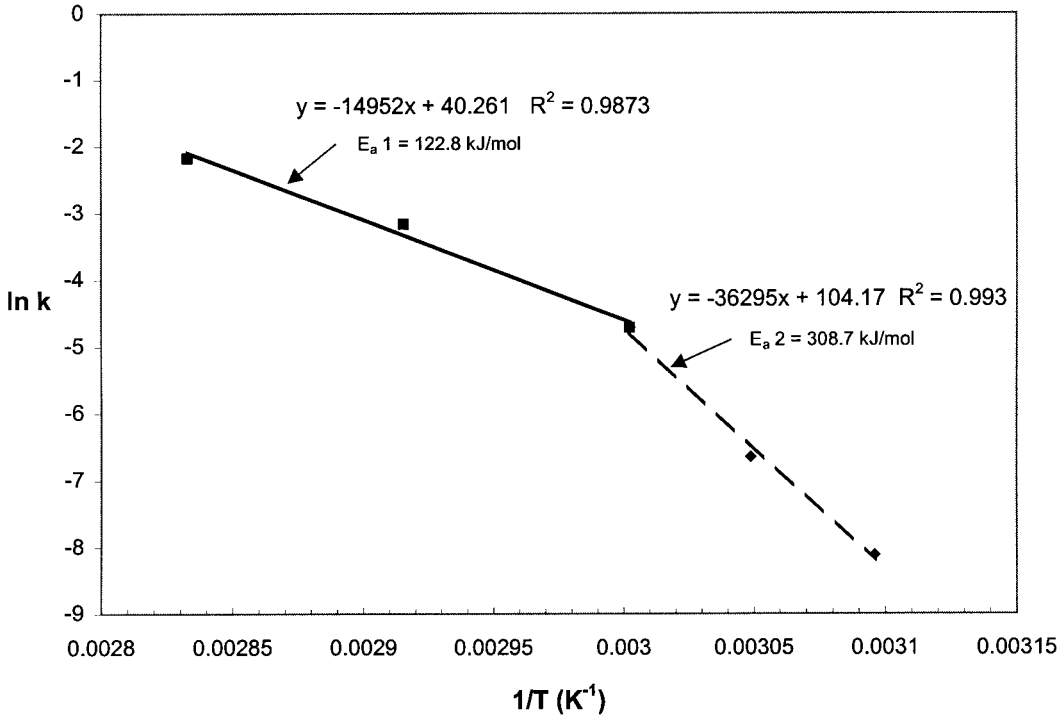

Figure 3. Arrhenius plot of the rate constants obtained for the dehydration of FC dihydrate.

dehydrated (B) component is given in eq. 2:

$$I_{j\mathrm{B}} = (k_{j\mathrm{B}} X_{\mathrm{B}})/\mu^*_{\mathrm{mat}} \qquad (2)$$

Assuming $X_{\mathrm{A}} + X_{\mathrm{B}} = 1$, from the ratio of eqs. 1 and 2, the weight fraction of the dihydrate, X_{A}, is solved as in eq. 3:

$$X_{\mathrm{A}} = I_{i\mathrm{A}}/(I_{i\mathrm{A}} + I_{j\mathrm{B}}(k_{i\mathrm{A}}/k_{j\mathrm{B}})) \qquad (3)$$

Define I°_{A} as the intensity of phase A when $X_{\mathrm{A}} = 1$ (i.e., the FC dihydrate main peak prior to drying) and I°_{B} as the intensity of phase B when $X_{\mathrm{B}} = 1$ (i.e., no detectable FC dihydrate peak) and assume that μ^*_{mat} remains constant; then $k_{i\mathrm{A}}/k_{j\mathrm{B}} = I^\circ_{\mathrm{A}}/I^\circ_{\mathrm{B}}$, and eq. 3 can be represented as in eq. 4:

$$X_{\mathrm{A}} = I_{i\mathrm{A}}/(I_{i\mathrm{A}} + I_{j\mathrm{B}}(I^\circ_A/I^\circ_B)) \qquad (4)$$

The mass absorption coefficient of the sample matrix will change as the sample is dried and unbound water is evaporated. However, the calculated mass absorption coefficients for the dihydrate and the monohydrate (using the atom mass absorption coefficients[11]), 17.6 and 17.8 cm^2/g, respectively, are sufficiently close relative to the errors in PXRD peak integration to consider μ^*_{mat} constant during the dehydration to the monohydrate. With a constant μ^*_{mat}, the need for an internal standard is avoided. With a single sample preparation and the dehydration performed at the X-ray diffractometer, errors due to changes in preferred orientation during drying are eliminated, minimizing the need for any method validation.

Using the strongest diffraction peaks for the crystalline dihydrate (a split peak centered around 6.2° 2θ) and the simply ordered monohydrate FC (5.0° 2θ), the weight fraction of the dihydrate was determined versus time of drying. Figure 5 shows the plot of the weight fraction of the dihydrate versus time at 50°C. The integrated peak data used to calculate Figure 5 is provided in Table 4.

Qualitatively, Figure 4 suggests that the dehydration of the dihydrate at 50°C produces a two-phase system comprised of a mixture of the crystalline dihydrate and the partially crystalline monohydrate. If the dehydration process involved a single-phase system where the crystalline material uniformly became more disordered with increased water loss, one should observe one set of diffraction peaks gradually shifting from their

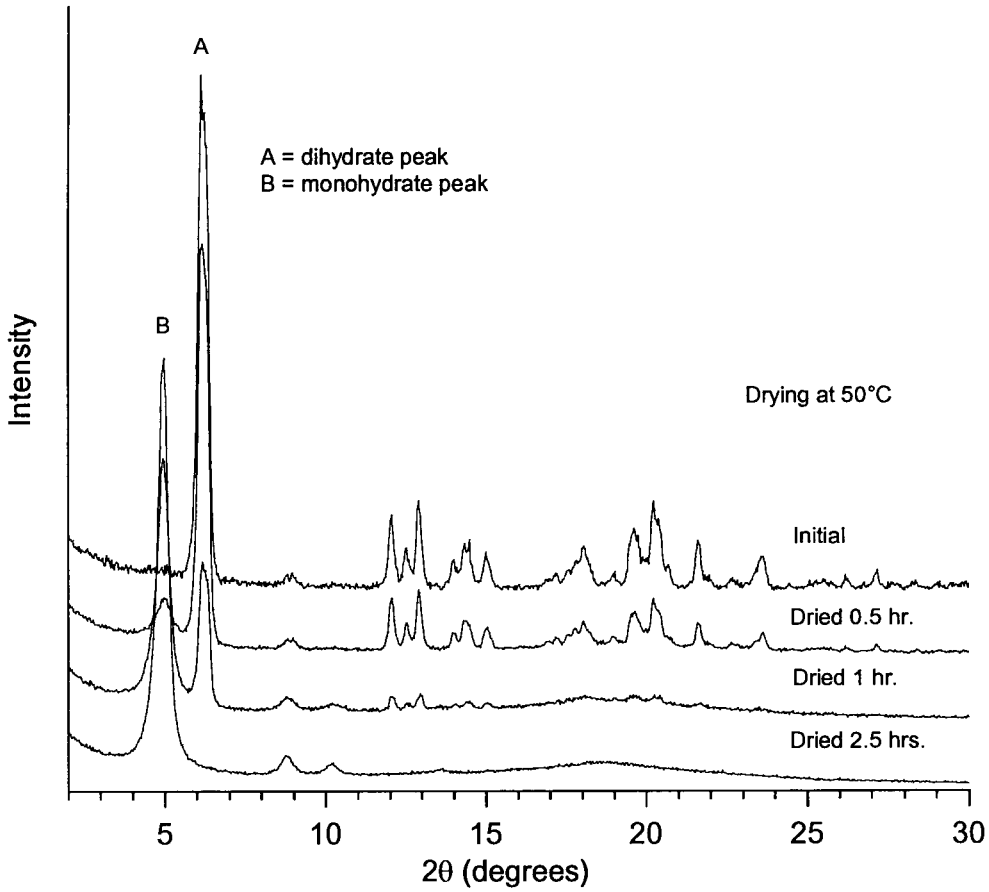

Figure 4. The powder diffraction pattern of FC dihydrate over time when exposed to 50°C.

original position to their final position after drying rather than observing (as we do) the separate dihydrate and the monohydrate peaks. In addition to the diffraction peaks in the 3–11° 2θ range for the monohydrate, a weak broad "halo" or hump in the baseline is observed around the 16–22° 2θ range. The weak broad "halo" represents an amorphous aspect of the monohydrate compared with that observed by the strong low-angle diffraction peak.

Further drying at 80°C produced an FC anhydrate, as confirmed by TGA, with a similar pattern as the monohydrate obtained by drying at 50°C. Additional drying at 120°C produced little change except for a slight sharpening of the diffraction peaks and slight shifts to higher *d*-spacings (lower 2θ), which were probably due to decreased unit cell density with increased temperature (see Figure 6). The PXRD pattern for the anhydrate in Figure 6 is consistent with the pattern for the anhydrous FC presented in an earlier work.[4] There are weak peaks in Figure 6 between 8 and 10° 2θ that were not observed in the prior work; the absence of these peaks is probably due to sensitivity differences between the PXRD instruments.

Dehydration/Rehydration Study Using PXRD

Duplicate dehydration/rehydration experiments were performed using the oven and humidity cabinet. Dehydration of the FC dihydrate to the anhydrate was complete after 40–45 min in the vacuum oven at 70°C, as indicated by the PXRD pattern (Figure 7). The appearance of the FC was changed little during the dehydration process. Both the dihydrate and the anhydrate consisted of white granular particles.

Exposing the anhydrate to 40°C/75% RH initially caused the material to become more disordered (Figure 7). After ~20–30 min at 40°C/75% RH, the sample became a clear, liquescent mass. As the material aged at 40°C/75% RH, the formation of the dihydrate crystalline phase was

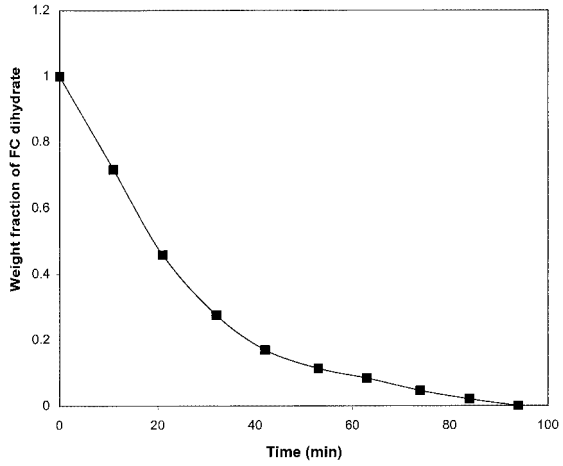

Figure 5. Plot of % crystalline FC dihydrate versus time when exposed to 50°C by quantitative PXRD analysis.

Table 4. Integrated XRD Peak Intensities

Drying time (min)	Form A (6.2° Split Peak) Dihydrate (Arbitrary Units)	Form B (5.0° Peak) Monohydrate (Arbitrary Units)
0	80830	0
11	51492	17400
21	33694	33938
32	20633	46130
42	13285	55331
53	8934	59547
63	7076	65602
74	3784	66422
84	1727	70896
94	0	69053

readily apparent both visually and by PXRD (Figure 7). The presence of an intermediate liquescent phase prior to crystallizing of the dihydrate suggests a solution-mediated rehydration process. Crystallization of the dihydrate appeared essentially complete after 190 min at 40°C/75% RH.

A second experiment using the same methodology produced similar results, however the crystallization of the dihydrate occurred more rapidly than in the first experiment. After 55 min at 40°C/75% RH, crystallization of the dihydrate appeared to be complete by PXRD.

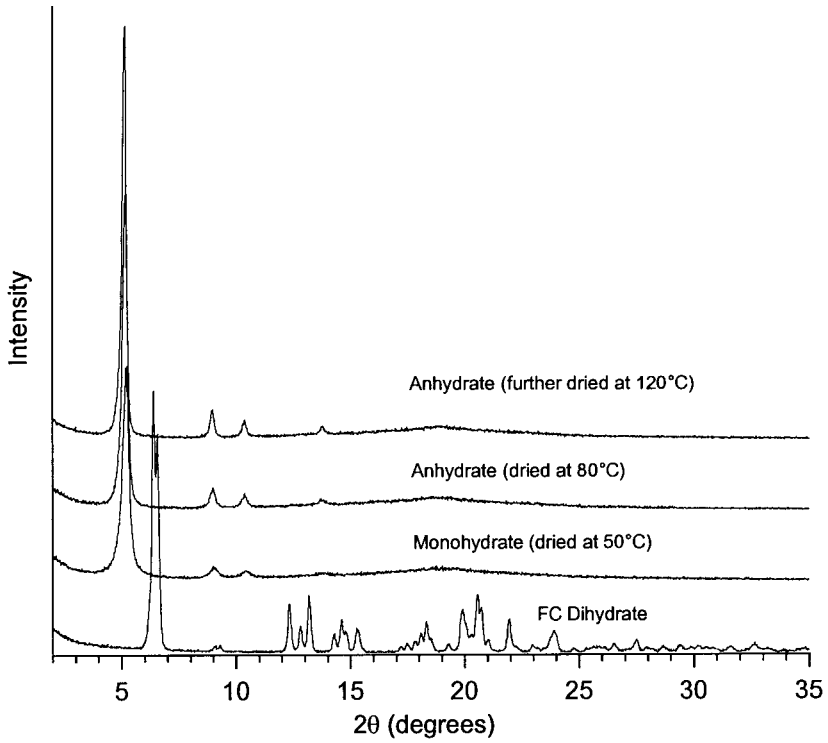

Figure 6. PXRD patterns of FC dihydrate, monohydrate obtained by drying at 50°C, anhydrate obtained by drying at 80°C, and anhydrate with further heating at 120°C.

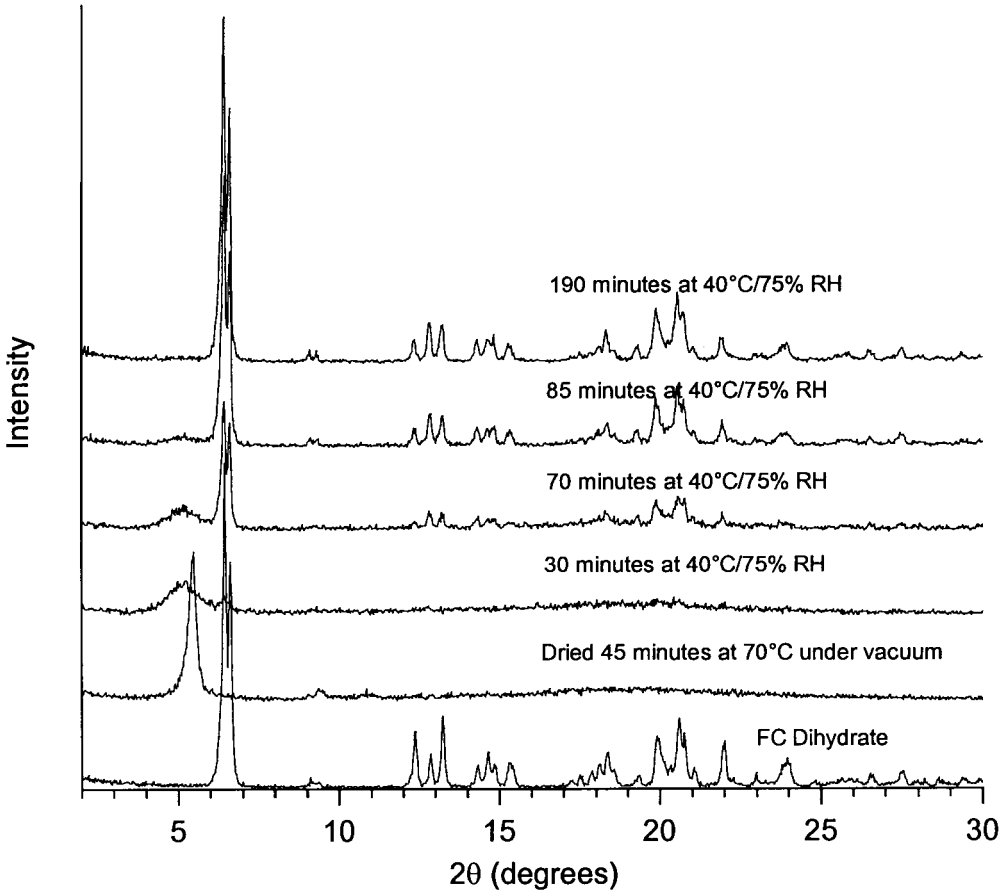

Figure 7. PXRD patterns showing the dehydration and rehydration of the FC when exposed to different conditions.

Duplicate dehydration/rehydration experiments were also performed using the hot stage/environmental chamber. For both experiments, dehydration of the dihydrate was complete after 10 min in the drying phase. Rehydration of the FC occurred much slower in the environmental chamber than it did in the humidity cabinet. The first experiment showed no evidence of the crystalline dihydrate after exposure to 40°C/75% RH for ~14.5 h. Some crystalline dihydrate was observed during the second experiment, but only after ~30 h at 40°C/75% RH. The experiment was carried out to 41.5 h, and crystallization of the dihydrate never went to completion. The observed difference in the rate of recrystallization between the environmental cabinet and the PXRD environmental chamber may be a consequence of static versus dynamic moisture introduction or due to differences in sample mass, geometry, or flow rate of the gas stream.

Single Crystal Results

The asymmetric unit for FC dihydrate is shown in Figure 8. The compound crystallized in a monoclinic lattice with a $P2_1/n$ space group (Table 1). The crystal structure is racemic with one *R*-enantiomer and one S-enantiomer of fenoprofen anion and two molecules of water per divalent calcium atom. In the asymmetric unit, one fenoprofen anion exhibited disorder, which was modeled by the crystallographer by two different atomic coordinates at 50% occupancy each for both the CH and CH_3 carbons. For viewing simplicity, only one set of carbon atoms is shown in Figure 8. Unlike the case for the reported structure of cromolyn sodium hydrates,[12] where the disorder in one of the sodium ions may contribute to the disorder and variable hydration nature, neither the calcium ions nor water molecules in our crystal structure are disordered. Except for

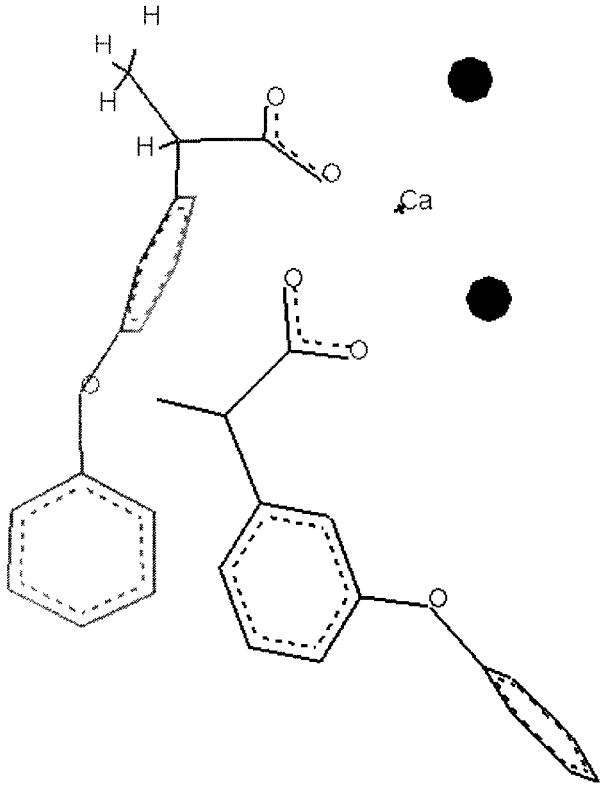

Figure 8. The asymmetric unit for fenoprofen calcium dihydrate. The oxygen atoms of the water molecules are represented by black balls.

the hydrogens on one $CHCH_3$ group, no hydrogens are shown because they were not refined in the structure. Thus, the water molecules are represented by their oxygen atoms only. Surrounding each calcium ion are six oxygens with a calcium–oxygen distance of ~2.3–2.4 Å. Two oxygens are provided by the water molecules and the other four oxygens come from four separate fenoprofen ions, as shown in Figure 9. Thus the two oxygens in any one carboxylate group coordinate to different calcium ions. In addition to the six oxygens within ~2.4 Å from a central calcium ion, there is a seventh oxygen from a FC group at 2.7 Å.

A search through the Cambridge Structural Database of calcium-containing compounds indicated that calcium is coordinated with 3 to 8 or 10 neighboring oxygens or nitrogens, with coordinations of 6 and particularly 8 being very common. If one water molecule per calcium ion is removed by drying, the stability of the hexacoordination state is lost producing a less ordered (less crystalline) material.

Because the hydrogen atoms of the water molecules were not refined during the single-crystal structure analysis, determining the extent of hydrogen bonding of water with the fenoprofen is difficult. Using the "ADD HYDROGENS" feature of Cerius2, hydrogens were added to each oxygen atom corresponding to water molecules at an OH bond distance of 0.85 Å. The positions of the inserted hydrogen atoms were then refined by two approaches. One approach involved assigning atom charges using the Charge Equilibrium method in Cerius2 and then minimizing the lattice energy with the Dreiding forcefield, v. 2.21, with the constraint that only the inserted hydrogen positions could change. The other atom positions and unit cell dimensions remained fixed. After minimization, the hydrogen bonds were calculated using the "CALCULATE H-BONDS" feature of Cerius2. In the other approach, the orientation of the hydrogen atoms were varied using the "3D SKETCHER" tool to establish optimum hydrogen bonding patterns (using the "CALCULATE H-BONDS" tool) between the water molecules and the carboxylate oxygens.

Using the energy minimization approach, one water molecule was involved in a hydrogen bond between a water hydrogen and a carboxylate oxygen and the other water molecule was not involved in any hydrogen bonding. Using the "manual" approach to optimize H-bonding, both water molecules appear to have similar hydrogen bonding opportunities (i.e., the strength of the hydrogen bonding should be similar). Thus, while the first approach suggests that one water molecule may be more tightly bound within the crystal structure due to limited hydrogen bonding, this suggestion is not confirmed by the "manual" approach. Because of the limitations in the Dreiding force field, the reliance on molecular mechanics calculations for optimizing hydrogen positions can be useful but not absolute. Ideally, the hydrogen positions should be refined from single-crystal X-ray or neutron diffraction. In addition, the distance between the water oxygen atoms and the calcium ions is about the same so that the extent of electrostatic attraction between the calcium cations and the electronegative water oxygens should be equivalent.

The one significant observable difference between the water molecules is their location. One water molecule (labeled by its oxygen atom as O42) is located between repeating carboxylate groups. The oxygen O42 atoms are represented as red balls in Figure 10. The other water molecule (labeled by its oxygen atom as O41) is located above/below the carboxylate groups, as shown as

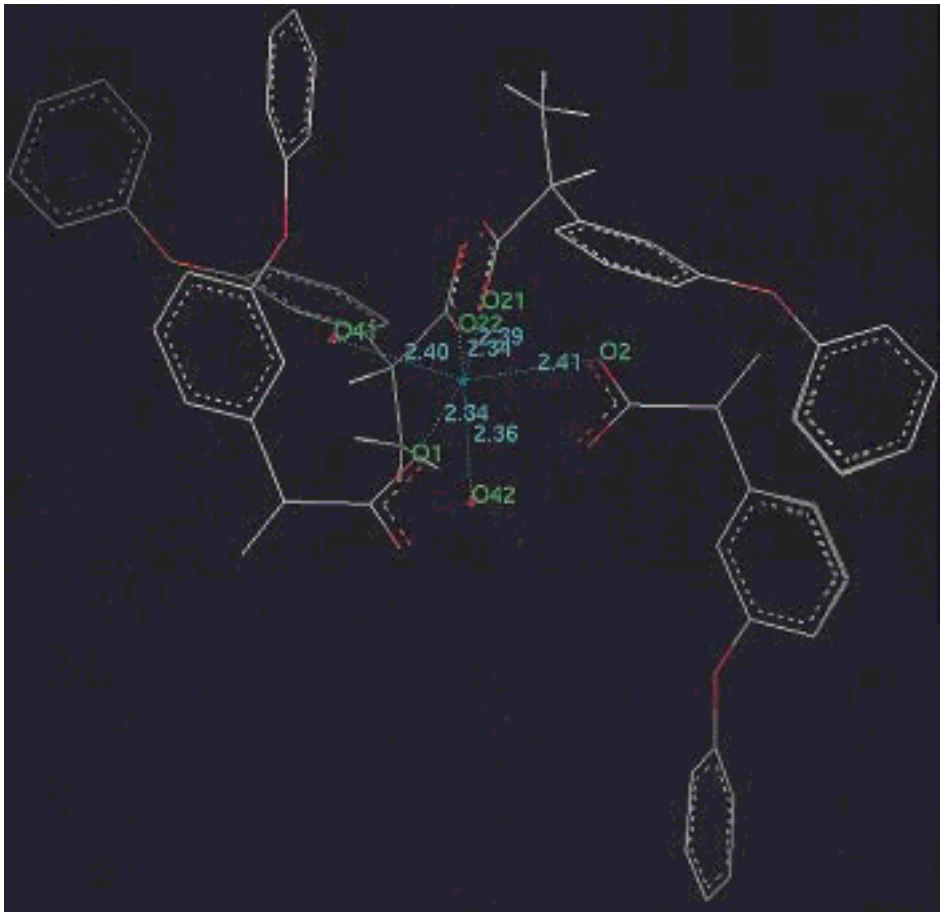

Figure 9. Coordination of calcium with oxygen atoms from four separate fenoprofen anions (O1, O2, O21, O22) and two distinct water molecules (O41, O42). Ca–O distances (Å) denoted in blue.

red balls in Figure 11. Visually, free pathways out of the crystal seem to exist along the b and c axes for the O41 water molecule and along the a and c axes for the O42 water molecule. However, using the Connolly Surfaces module in Cerius2 to calculate solvent channels, no such channels large enough to fit water molecules are observed, suggesting there is insufficient room for the dihydrate crystal structure to lose water without disrupting the crystal. At elevated temperatures, the crystal unit cell may expand allowing egress of water.

Thus, during drying, water at one crystallographically distinct position is probably preferentially removed relative to water at the second position. Based on the hydrogen bonding calculations of the energy minimized, the dihydrate structure as well as the location of the O42 water lying in between repeating polar carboxylate groups, the O41 water, located in a slightly less polar region of the crystal, is probably preferentially lost during drying. However, it takes some energy to remove this water because of the electrostatic attraction between the calcium ions and water's oxygen atom where the lattice favors the hexacoordination sphere for calcium.

Based on the crystal structure analysis, the presence of two "modes" of dehydration process as suggested by PXRD and thermal analysis data is confirmed. One water is lost from a crystalline matrix followed by loss of a second water from a partially crystalline phase.

Figure 12 shows a staggered overlay of the experimental with the simulated PXRD pattern (the latter calculated from the crystal structure). Indexing of the experimental PXRD pattern as well as Rietveld refinement (DBWS) of the crystal structure indicated there as an approximate -0.1 degree 2θ error in the experimental PXRD pattern, probably due to negative sample displacement error. The experimental PXRD pattern has been offset to compensate for the 2θ error in Figure 12. Rietveld refinement indicated that the

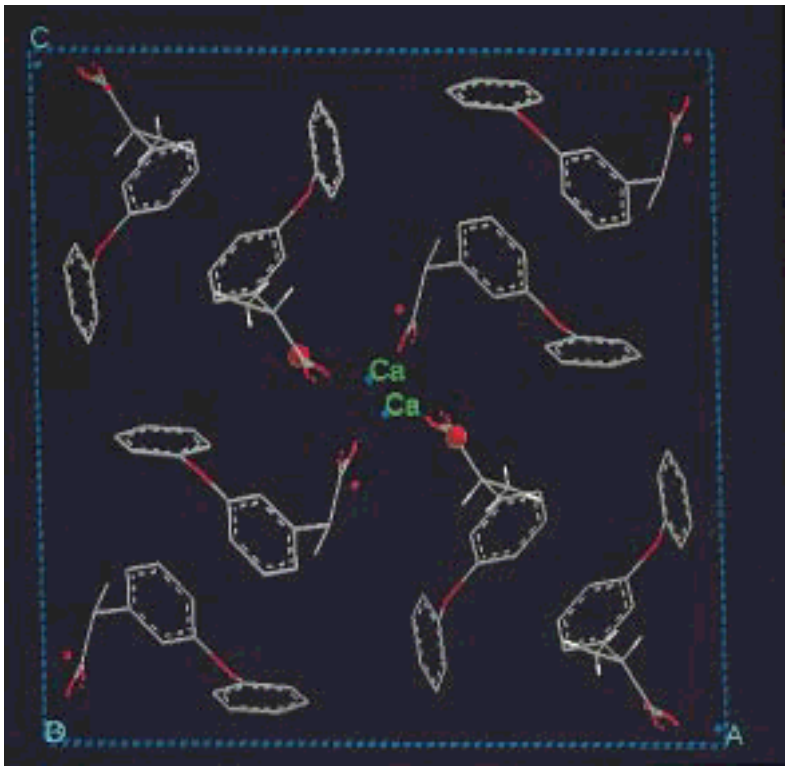

Figure 10. The O42 oxygen atom from water is represented by a red ball. Other oxygens, carbons, and hydrogens (not all shown) are in red, gray, and white colors, respectively. The view is down the b crystal axis.

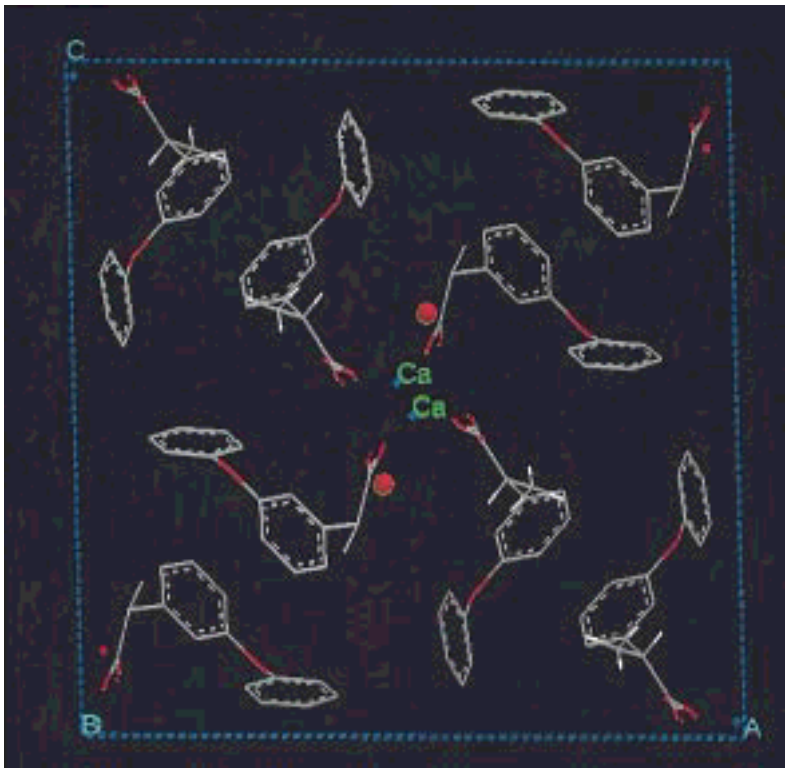

Figure 11. The O41 oxygen atom from water is represented by a red ball. Other oxygens, carbons, and hydrogens (not all shown) are in red, gray, and white colors, respectively. The view is down the b crystal axis.

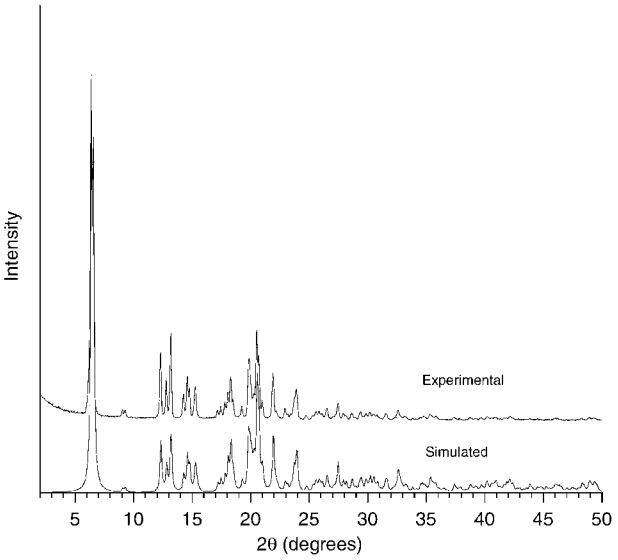

Figure 12. Overlay of experimental (top) and simulated (bottom) XRD patterns.

unit cell dimensions at $-100°C$ (determined by single-crystal XRD) and room temperature (from PXRD) are the same within experimental error.

The crystal structure of the dihydrate was "computationally" dehydrated by first adding missing hydrogens and minimizing the crystal structure while maintaining the unit cell parameters and other atom positions, as discussed previously. From this "refined" structure, one water molecule was removed from the crystal structure (to make the monohydrate), and the resulting structure energy was minimized with no atom and unit cell constraints. Both Dreiding and Universal force fields were tried. The process was repeated by removing the other water molecule from the dihydrate crystal structure to make another monohydrate. Finally, both waters were removed (fully dehydrated structure) and the dehydrated structure minimized. The PXRD patterns were calculated for all minimized structures. Because energy minimization will not "convert" a crystalline structure to a partially crystalline structure, it was not surprising that none of the calculated PXRD patterns were similar to the experimental patterns for the partially dried monohydrate or fully dried anhydrous material monohydrate. Also, the anhydrates are not dehydrated hydrates but are simply ordered structures with possible remnants of the original crystalline dihydrate structure.

CONCLUSIONS

Arrhenius plot (natural logarithm of the dehydration rate constant versus the inverse of the absolute temperature) from isothermal TGA suggests a break that indicates two "modes" of dehydration process for FC dihydrate. Using quantitative PXRD, the loss of only 1 mol of water per mole of FC dihydrate was required for the material to convert to a partially crystalline phase. Both water molecules are required to maintain the original crystalline structure. Presumably the first loss of water starts from a crystalline state followed by loss of the second water from a partially crystalline state. Single-crystal XRD analysis confirmed the dihydrate stoichiometry and revealed the crystal packing arrangement in FC. The oxygens from the fenoprofen anions and from the water molecules served to fill the hexacoordination sphere for calcium. Analysis of the structure data indicated the two water molecules were inequivalent, with one water located in between repeating carboxylate groups. Analysis of the relative amounts of hydrogen bonding for the two water molecules is inconclusive but suggests that the water located in between the carboxylate groups is in a better position for hydrogen bonding to the carboxylate moiety compared with the other water molecule. The rehydration process is not the reverse of the dehydration process. The rehydration of the anhydrous FC goes through a solution-mediated process prior to crystallizing as the dihydrate.

ACKNOWLEDGMENTS

The authors thank Sean Lynn, Glaxo Wellcome Research and Development (Stevenage, UK), for performing the coordination number search of calcium compounds in the Cambridge Structural Database and Peter White, X-ray Crystallographic Facility, Chemistry Department, UNC, for providing the crystal structure of calcium fenoprofen. The authors also thank one of the reviewers for helpful comments regarding comparisons of our work with that of prior authors (Sathe and Moore) as well as all of the reviewers for comments that help strengthen the manuscript.

REFERENCES

1. Berge SM, Bighley SD, Monkhouse DC. 1977. Pharmaceutical salts. J Pharm Sci 66:1–19.

2. Forbes RT, York P, Fawcett V, Shields L. 1992. Physicochemical properties of salts of p-aminosalicylic acid. I. Correlation of crystal structure and hydrate stability. Pharm Res 9:1428–1435.
3. Hirsch CA, Messenger RJ, Brannon JL. 1978. Fenoprofen: Drug form selection and preformulation stability studies. J Pharm Sci 67:231–236.
4. Sathe R, Moore S. 1995. Dehydration and hydration kinetics, phase change, solubility and dissolution behavior of fenoprofen calcium. Drug Dev Ind Pharm 21(16):1887–1894.
5. Florey K, editor. 1977. Analytical Profiles of Drug Substances and Excipients, Vol. 6. New York: Academic Press, pp. 161–182.
6. Gabe EJ, Le Page Y, Charland J-P, Lee FL, White PS. 1989. NRCVAX an interactive program system for structure analysis. J Appl Crystallogr. 22:384–387.
7. Buckner C, Kidd C, Long S, Varlashkin P, Zhu H. 1999. Environmentally controlled sample stage for Scintag's six-position XRD sample changer. Powder Diffraction 14(4):296–299.
8. Sharp JH, Brindley GW, Achar BNN. 1966. Numerical data for some commonly used solid state reaction equations. J Am Ceram Soc 49:379–382.
9. Byrn SR. 1982. Solid state chemistry of drugs. New York: Academic Press, Inc.
10. Monkhouse DC, Van Campen L. 1984. Solid state reactions- Theoretical and experimental aspects. Drug Dev Ind Pharm 10:1175–1276.
11. Cullity BD. 1978. Elements of X-Ray Diffraction, Appendix 8. Reading, MA: Addison-Wesley Publishing Company, Inc.
12. Chen LR, Young Jr. VG, Lechuga-Ballesteros D, Grant DJW. 1999. J Pharm Sci 88:1191–1200.